COMPARING *k-ε* MODELS ON PREDICTIONS OF AN IMPINGING JET FOR VENTILATION OF AN OFFICE ROOM

Huijuan Chen[1,2], Bahram Moshfegh[1,2]
[1]Department of Building, Energy and Environmental Engineering, Faculty of Engineering and Sustainable Development, University of Gävle, Gävle, Sweden
[2]Division of Energy Systems, Department of Management and Engineering, Linköping University, Linköping, Sweden

Abstract

The objective of this study is to compare the performance of different *k-ε* models, i.e. the Standard *k-ε*, the Renormalization Group (RNG) *k-ε*, and the Realizable *k-ε*, with a two-layer model for the prediction of the mean velocity field and the temperature pattern from a newly designed impinging jet supply device for ventilation of an office room. The numerical predictions are validated against the detailed experimental measurements.

The experimental investigation was performed in a test room with the dimensions 4.2×3.6×2.5 m, as a mock-up of a single-person office. Detailed velocity and temperature field measurements including the comfort zone and the jet developing region along the floor were carried out. The in-house made single-sensor hot-wire probe and the thermocouple are measuring instruments used to investigate the mean velocity, turbulence intensity and temperature. The boundary conditions for Computational Fluid Dynamics (CFD) study are obtained from the same set-up measurement.

The results mainly consist of the flow field presentation, i.e., the velocity and temperature profiles in the comfort zone and the jet developing region along the floor. The comparisons between the results from the three versions of the *k-ε* models and measurements show generally satisfactory agreement, and better consistency is observed at the free jet region and the wall jet region that farther from the impingement zone. Among the three tested turbulence models, RNG shows the best overall performance.

Keywords: CFD, Impinging jet ventilation, Turbulence model, Wall jet, Measurement

1 Introduction

Heating, Ventilation and air-conditioning (HVAC) system is of vital importance for buildings, not only to provide acceptable thermal conditions and air quality for occupants, but also with regards to energy usage. Meanwhile, ventilation strategies based on different air distribution methods have major impacts on the thermal environment and energy performance, see Karimipanah et al. (2008). Due to the growing concern about global warming and energy shortages, utilizing energy in a more efficient way is increasingly promoted. Therefore, there are incentives to develop effective ventilation methods able to fulfil the requirements for thermal comfort and indoor air quality while using less energy.

The impinging jet concept was introduced and proposed as a new ventilation strategy, termed Impinging Jet Ventilation (IJV) (Karimipanah and Awbi 2002), which is based on the principle that a high momentum air jet discharged downwards, strikes the floor and spreads over it, thus distributing the fresh air along the floor in the form of a very thin shear layer. This method enables the air jet to overcome the buoyancy force generated from heat sources and reach farther regions. The flow field of the impinging jet is characterized as the combination of three regions, i.e. free jet region, impingement region and wall jet region, as illustrated in Figure 1. For the air conditioning application, the wall jet region is of greatest concern, since the jet running directly into the occupied zone might cause a

draught sensation due to the high velocity. Therefore, the jet discharge height and the supply airflow rate should be designed properly.

To achieve the optimal air distribution control and create the desired indoor environment, detailed information about air velocity, temperature, turbulence and contaminant concentration within the enclosed space needs to be obtained. Nowadays, numerical simulation by means of Computational Fluid Dynamics (CFD) is a promising tool extensively used for room air movement prediction, and successful simulation would have great benefit for HAVC system design. However, it is necessary to ensure the reliability of the CFD model by comparing with experimental data, since the uncertainties introduced from turbulence modeling, boundary condition specifications and air supply diffuser simplification, etc. would influence the accuracy of computational results. Therefore, the procedure regarding CFD validation was developed by Chen and Srebric (2002).

The purpose of this study is to investigate the flow features produced by a newly designed wall-mounted Impinging Jet (IJ) device as well as evaluate the performance of the implemented k-ε models by comparing with measurements. The comfort zone and the jet developing region along the floor are of interest for analyzing the mean velocity and temperature distributions. The extensive numerical parametric study will be performed in the near future, which aims at analyzing the effects of the jet discharge height, the supply airflow rate and the diffuser geometry on the resulting room airflow configuration.

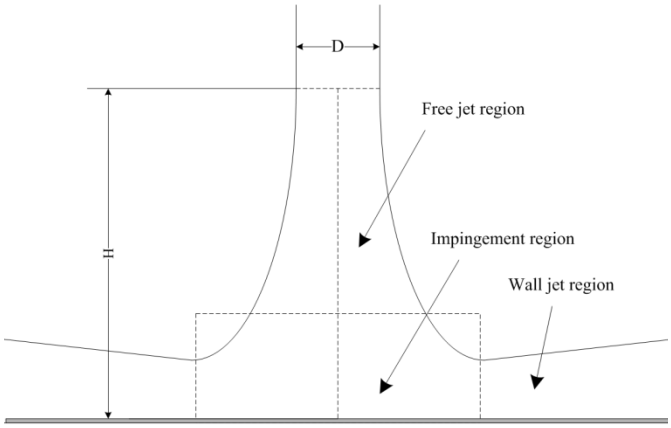

Figure 1. Flow regions of an impinging jet

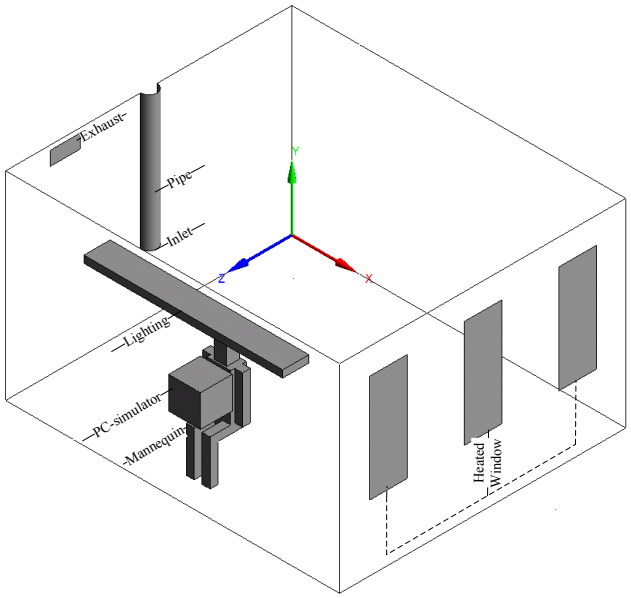

Figure 2. Computational domain

2 Computational set-up and numerical scheme

2.1 Physical model and boundary conditions

The physical model under consideration is a test room furnished like a single-person office, with the dimensions 4.2×3.6×2.5 m. Different components are used to simulate the summer working environment and generate the heat load of 35 W/m^2, i.e. PC-simulator (120 W), mannequin (95 W), lighting (144 W), heated floor (150 W), and three heated windows simulated by heating foil sheets (3×35W), see Figure 2. The IJ device and exhaust opening are installed on the same side wall. In addition, a cooling panel beam is installed and covers most part of the ceiling to supplement the cooling effect from IJ ventilation.

The boundary conditions are specified as follows: At the inlet (the jet discharged section), the measured y-component velocity profile, V, is imposed, with the measured average temperature 16.2 °C.

The distributions of turbulence quantities for k and ε are determined by using the following formula (Ansys Fluent Users' Guide, 2009).

$$k_{in} = 1.5(V_{in}T_u)^2 \quad (1)$$

$$\varepsilon_{in} = C_\mu^{\frac{3}{4}} k^{\frac{3}{2}}/l \quad (2)$$

Where, V is the y-component velocity at the inlet, and l is a length scale given by $l = 0.07D$, D is the hydraulic diameter for the jet discharged section. At the exhaust, the pressure outlet is used that assumes the gauge pressure is zero. All the internal surfaces of the room are set as non-slip walls with uniform temperatures obtained from measurements, and the rest of the heated objects are provided with the fixed heat flux.

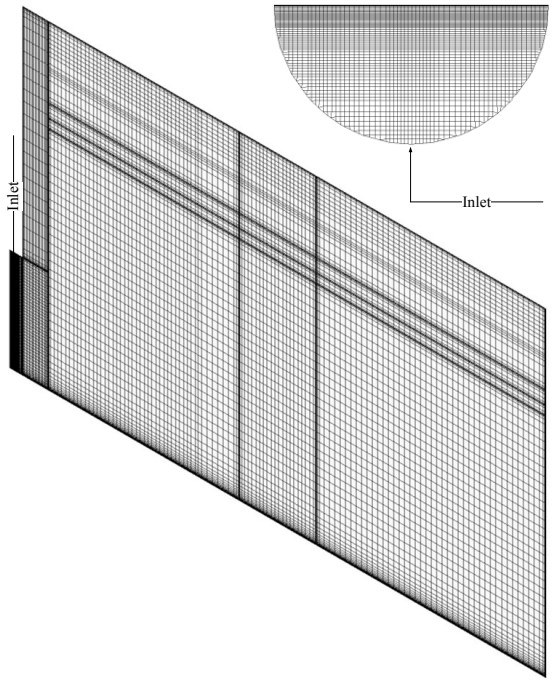

Figure 3. Mesh configurations in the vertical middle plane as well as at inlet

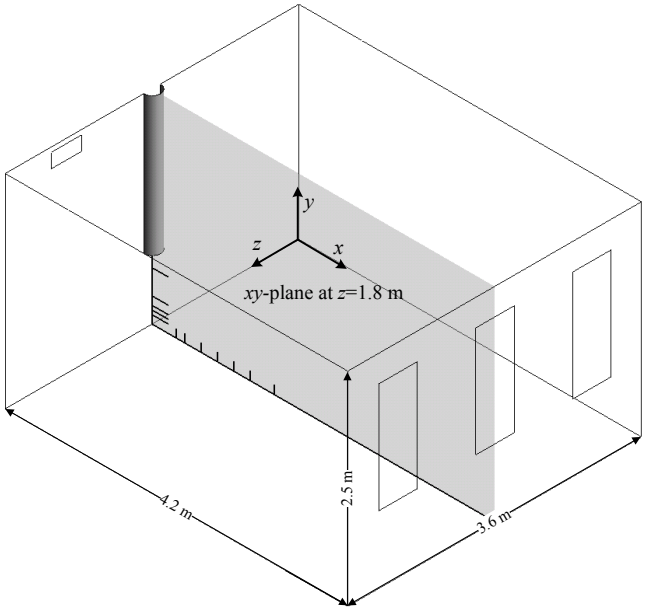

Figure 4. Measuring locations

2.2 Governing equations and turbulence modelling

The airflow field and temperature patterns resulting from the IJ device in the test room are simulated by numerically solving the steady-state, three-dimensional, incompressible and time-averaged Navier-Stokes and energy equations. Turbulence is modeled by means of various levels of two-equation k-ε models, i.e. the Standard k-ε, the RNG k-ε and the Realizable k-ε model. For details about the mathematical formula description of the three versions of the k-ε models, see Moshfegh and Nyiredy (2004). The standard k-ε model is well documented and widely used; it requires less computational effort and is more easily converged. The RNG differs from the standard k-ε model mainly in the additional term introduced in the ε-equation, which defines a parameter that is the ratio between the time scales of the turbulence and the mean flow, thus making the RNG model superior for responding to the feature of rapid strain and streamline curvature compared to the standard k-ε model. For the realizable k-ε model, it satisfies certain mathematical constraints on the Reynolds stresses, which is consistent with the physics of turbulent flows, such as ensuring the normal Reynolds stress is positive by removing the unphysical negative values. This is achieved by allowing $C_\mu$to vary as a function of the mean strain, rotation and turbulence field. The turbulent heat flux is modeled by the eddy-viscosity hypothesis. The buoyancy effect is included in the momentum equation, and the fluid density is defined by the incompressible ideal gas law, indicating that the density only varies with

temperature. Due to the presence of the heat sources, the radiation heat transfer is taken into account and simulated with the Discrete Ordinate (DO) model, see Ansys Fluent Users' Guide (2009).

2.3 Computational grid and near wall treatment

Airpak 3.0.16 (Airpak, 2003) is chosen as pre-processor to construct the three-dimensional geometry and generate mesh, and the configuration of the semi-elliptical pipe is imported from ICEM CFD 12.1 via IGES file (Ansys ICEM CFD, 2009). The computational domain is dominated by the hexahedral elements, and the mixed elements only exist around the inlet region. In order to avoid the unnecessary fine mesh projected from the inlet and heated objects into the whole computational domain, the non-conformal mesh is applied to enclose those objects. To determine the necessary grid resolution for independent solutions, three grid schemes with different densities and shapes are tested by the RNG model; the grid information is listed in Table 1. Comparing the predicted values from the three meshes, no appreciable difference is observed between the latter two finer meshes, but larger deviation is noticed from the first, coarser one. The compared results will be presented in the section on results and discussion. Considering the computational effort and the reasonable accuracy, the grid with 5,683,631 cells is assumed to be sufficient. The represented mesh configuration for grid 2 is displayed in Figure 3.

Non-uniform grid distribution scheme is used for efficiently covering the whole computational domain. Finer mesh is placed adjacent to the wall and the region with the steep gradient of variables. The mesh is refined enough near the solid walls by keeping the $y+$ to be less than one (except in the region close to the heat sources, where the maximum $y+$ is around 1.7) in order to solve the all boundary layer with the two-layer model.

Table 1. *Grid information*

Cells	Grid 1	Grid 2	Grid 3
Total	3,842,906	5,683,631	7,500,620
Inlet	937	3,485	937

2.4 Numerical details

The finite-volume solver Fluent 12.1.4 (Ansys Fluent, 2009) is used to simulate the airflow and temperature fields with a segregated scheme and the SIMPLE algorithm solves the pressure-velocity coupling. Regarding discretization, the non-linear terms are calculated with Second-order upwind scheme and the viscous terms with the Second-order central scheme, and pressure is discretized with PRESTO! (PREssure STaggering Option) scheme. The local criterion for numerical convergence, i.e. the maximum relative difference between two consecutive iterations for local variable p, u, v, w, k, and ε is less than 10^{-3}. The convergence criterion regarding energy is that the normalized residual falls less than 10^{-8}. In addition, the error for the overall mass flow and heat flux balances have been calculated and are less than 0.03 % and 0.3 %, respectively.

3 Experimental procedure

The measurements were performed at the Laboratory of Ventilation and Air Quality at the Centre of Built Environment, University of Gävle, Sweden. The test room was with the approximate identical set-up as studied in CFD. The air was supplied through a semi-elliptical 1.51 m long pipe, and discharged from the outlet with the area of 0.0166 m^2 at the height of 0.8 m above the floor. To create better inlet boundary conditions for numerical simulation, an extra pipe 1.0 m long was used to connect the supply duct with the IJ device for delivering more uniform flow. The supplied airflow rate was regulated to 0.025 m^3/s and measured by orifice plate, with accuracy of ±5 %. The detailed flow field measurements were conducted at different locations both in the comfort zone and the jet

developing region along the floor. The typical measuring lines are displayed in Figure 4. The velocity measurements were performed using a 5μm platinum-coated tungsten sensor and a Dantec 56C01 anemometer system with a 56C17 bridge. The hot-wire was calibrated in the velocity range 0.2 – 2.5 m/s and the data were fit to a 4th order polynomial. Calibration was performed at two different temperatures thus allowing for temperature correction of the velocity data. Meanwhile, a small thermistor was positioned close to the anemometer probe to measure the air temperature. The velocity was measured over 2 minutes with the sampling rate of 100 Hz. The accuracy for temperature is ±0.1 °C, and the accuracy for velocity measurements is estimated to ±5% or ±0.03 m/s, whichever is greatest. In addition, the air temperatures as well as the internal wall surface temperatures were measured by thermocouples with an accuracy of ±0.1 °C. In this study the average room air temperature was controlled around 21.0 °C. In addition to the measurements concerning the IJ characteristics, the mean velocity, V, and turbulence intensity, T_u, profiles were captured by traversing the sensors through the region 4 mm beneath the supply exit section and covering the whole supply projected area. Figure 5 (a) and (c) show the contour plots of V velocity and turbulence kinetic energy at the inlet, which are generated by the constant interpolate method by CFD based on the specified point profiles from measurement. The represented V velocity and the corresponding turbulence intensity T_u profiles across the inlet are shown in Figure 5 (b), which is at a distance of 0.052 m from the bottom of the pipe. The top-hat V velocity profile indicates that the fully developed flow condition is reached at the jet exit section. All the measurements were carried out under steady-state condition.

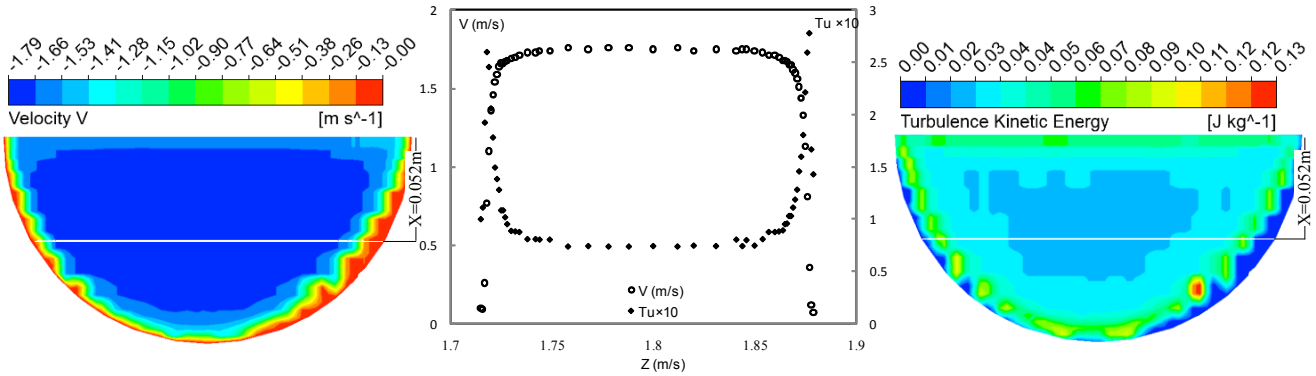

(a) (b) (c)

Figure 5. Boundary conditions for the velocity profile, V, (a) and the turbulence kinetic energy profile (c) used for the numerical simulation based on the measured values at 4 mm beneath the supply exit section of the impinging jet. (b): the represented measured velocity V and turbulence intensity Tu profiles at a distance of 0.052 m from the bottom of the pipe.

4. Results and discussion

4.1 Grid independency study

To distinguish the error induced from turbulence modelling, grid independence is examined first. Figure 6 shows the maximum velocity decay along the centerline of the floor. It can be seen that the predicted maximum velocities from the three meshes are quite close, which indicates the first mesh is still fine enough at the region very close to the floor. However, some differences are presented when comparing the velocity profiles at one specified location, as shown in Figure 7. Grid 1 smears the steep velocity gradient to some extent at a higher level above the floor, while the profiles from grid 2 and 3 show a very similar form. Therefore, these two comparisons confirm the choice for grid 2.

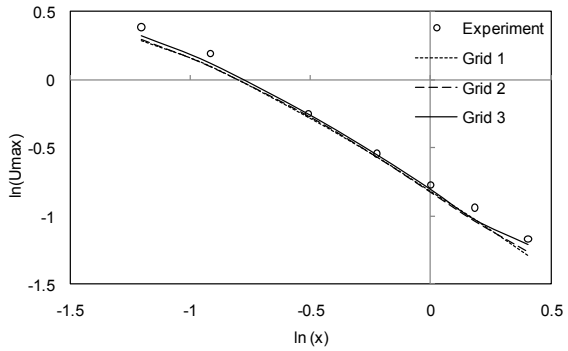

Figure 6. Maximum velocity decay along the centerline of the floor

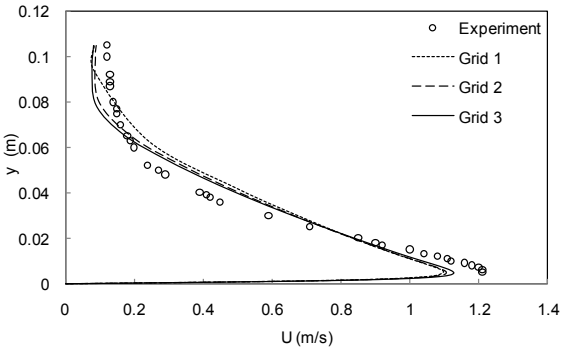

Figure 7. Velocity profiles at x= 0.4 m and z = 1.8 m

4.2 Comparison of the jet velocity and temperature profiles

The simulation results from the three *k-ε* models are compared with the experimental data in terms of the mean velocity and temperature distributions. Figure 8 presents the comparison results at two locations below the diffuser in the comfort zone. The variation of the velocity profiles at different heights manifests the process of jet decaying as it is approaching the floor. The comparative analysis indicates that all the *k-ε* models are able to capture the velocity and temperature distributions satisfactorily according to the experimental findings. However a slightly over-predicted velocity is presented near the inlet wall (x = 0 m), at the height y = 0.6 m, which is probably due to the specified inlet velocity profile lacking the information of the sharp velocity gradient close to the bottom of the pipe. Concerning the thermal field, a small temperature discrepancy between the prediction and measurement is exhibited, which is under-predicted up to 0.5 °C and clearly shown at the location of y = 0.1 m. This deviation can be explained as the result of the under-predicted surrounding air temperature.

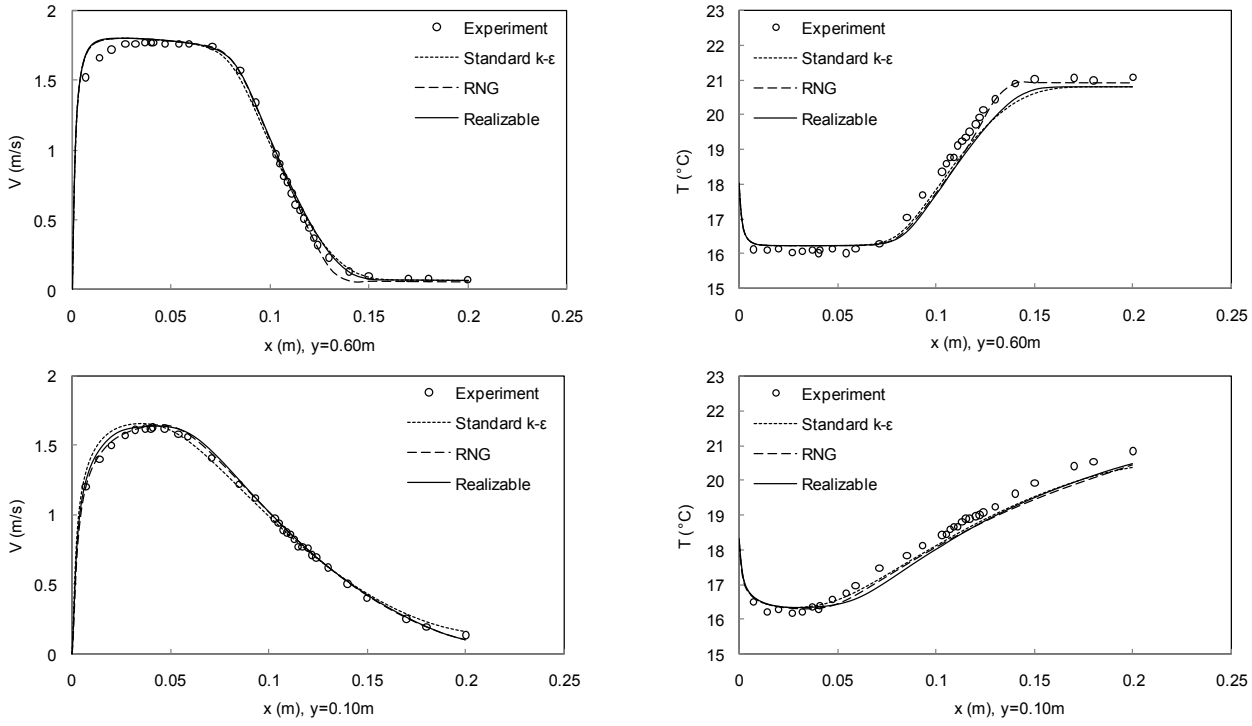

Figure 8. Horizontal velocity and temperature profiles at two heights above the floor in the xy-plane at z = 1.8 m (see Figure 4)

Besides comparing the jet profiles beneath the inlet, analyzing the wall jet behaviour along the floor is more substantial for validating the turbulence model. Figure 9 compares the mean velocity and temperature profiles with measurement at two downstream distances from the inlet wall along the centerline of the floor. Since the wall jet generated by IJ principle is rather thin, the results from both the measurements and CFD are particularly focused on the near wall region. At the location of x = 0.4 m, none of the k-ε models either captures the tendency or predicts the magnitude of the velocity accurately. The worst result is from the Standard k-ε model, and the closest agreement is obtained from RNG. The possible explanation is that the implemented two-equation k-ε models are unable to accurately predict the impingement region of the flow field, which is attributed to the excessively predicted kinetic energy in the vicinity of the stagnation point. A study by Behnia et al. (1998) has shown that in the stagnation region, the k-ε model significantly over-predicts the local Nusselt number. Therefore, in this study, the predicted unrealistic high kinetic energy near the stagnation point is retained until further downstream, i.e. at x = 0.4 m and z = 1.8 m, thus enhancing the mixing of the shear layer with the surrounding air, which results in the thicker jet profile and consequently reduces the local maximum velocity. Farther from the impingement zone, i.e. at x = 1 m and z = 1.8 m, the flow feature becomes relatively simple and the flow field is mainly influenced by the buoyancy force, and all the velocity predictions show a good consistency with the experimental data.

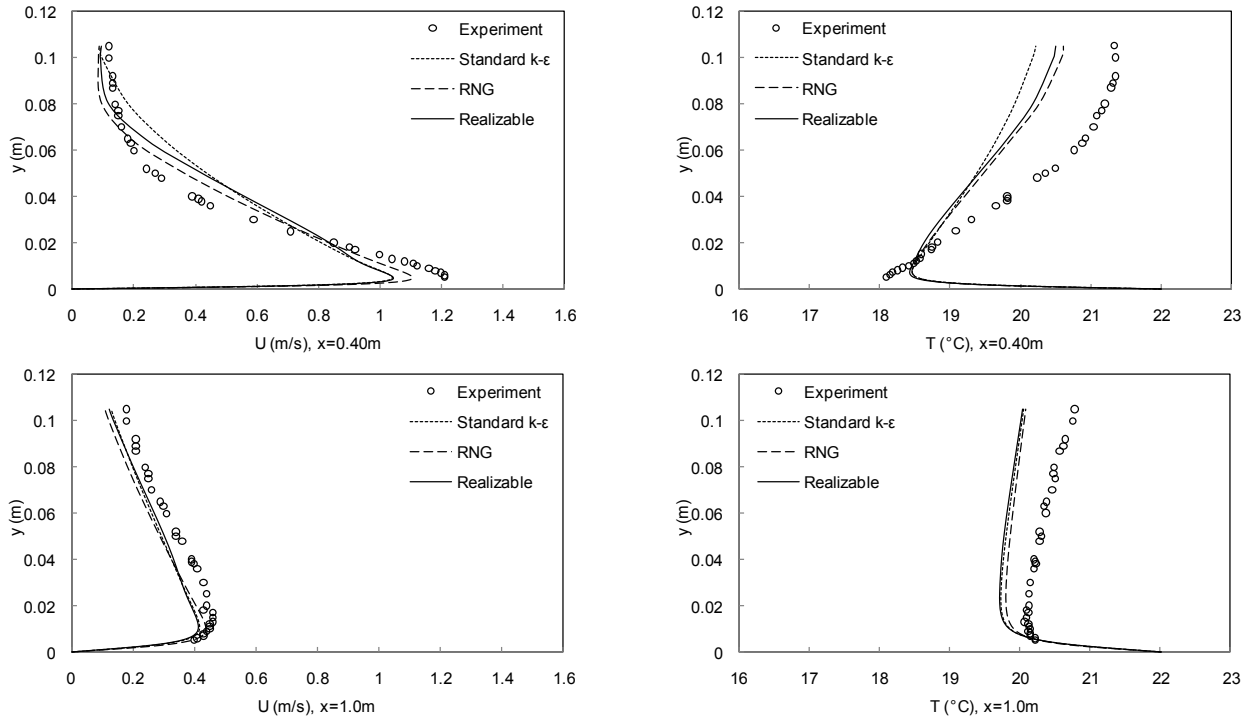

Figure 9. Vertical velocity and temperature profiles at two locations from the inlet wall in the xy-plane at z = 1.8 m (see Figure 4)

Concerning the thermal field of the wall jet, the temperature discrepancy between the CFD and measurement is presented in Figure 9. The deviation with measured data near the floor shrinks as it moves away from the inlet wall, which can be explained as the consequence of the imposed uniform floor temperature. At a higher level above the floor, the temperatures are under-predicted by all the turbulence models corresponding to the experimental findings, which may be caused by the lower predicted average room temperature. Since during the measurement, the surrounding environment of the test room in the lab is warmer, additional heat flux may be transmitted into and contribute to heating up the test room. However, this extra heating effect has not been taken into account by the thermal boundary conditions as currently provided. Even so, the maximum temperature discrepancy

between the RNG model and measured data is limited to 0.75°C. The predictions from RNG show the closest agreement, which is slightly better than the Realizable model.

4 Conclusion

In the present study, three two-equation *k-ε* turbulence models are evaluated in predicting the airflow pattern and thermal behavior of IJ ventilation of an office. The comparisons between the simulation results and measured data are made at different locations within different flow regions of IJ. The results indicate that all the tested *k-ε* turbulence models can capture the general flow feature satisfactorily, and better performance is observed at the free jet region and the wall jet region that farther from the impingement zone. Among the three tested turbulence models, RNG shows the best overall performance. In addition, the deviation between the CFD prediction and measurement close to the impingement region reveals that a better turbulence model should be used for handling the complicated flow feature.

Acknowledgments

The authors greatly acknowledge the financial support from KK Foundation, System Air AB, Kraft and Kultur AB and the University of Gävle. The authors sincerely thank Mr. Hans Lundström for his technical assistance on measurements and Dr Mathias Cehlin for his valuable help through study at the University of Gävle, Gävle, Sweden.

References

Airpak 3.0 (2007) User's Guide, Fluent Inc.

Ansys Fluent 12.1 (2009) User's Guide, ANASYS Inc.

Ansys ICEM CFD 12.1 (2009) User Manual, ANASYS Inc.

Behnia, M. Parneix, S. and Durbin, P.A. (1998) *Prediction of heat transfer in an axisymmetric turbulent jet impinging on a flat plate*, International Journal of Heat and Mass Transfer, Volume 41, 1845-1855.

Chen, Q. and Srebric, J. (2002) *A procedure for verification, validation, and reporting of indoor environment CFD analysis*, International Journal of HVAC&R Research, Volume 8, 201–216.

Karimipanah, T. and Awbi, H.B. (2002) *Theoretical and experimental investigation of impinging jet ventilation and comparison with wall displacement ventilation,* Building and Environment, Volume 37, 1329–1342.

Karimipanah, T. Awbi, H.B. and Moshfegh, B. (2008) *The air distribution index as an indicator for energy consumption and performance of ventilation systems*, International Journal of Human-Environment System, Volume 11, 77-84.

Moshfegh, B. and Nyiredy, R. (2004) *Comparing RANS models for flow and thermal analysis of pin fin heat sinks,* Proceedings of the 15th Australasian Fluid Mechanics Conference, December 2004, Sydney, Australia.